

Learning with Diversification from Block Sparse Signal

Yanhao Zhang, Zhihan Zhu, Yong Xia

Abstract—This paper introduces a novel prior called **Diversified Block Sparse Prior** to characterize the widespread block sparsity phenomenon in real-world data. By allowing diversification on variance and correlation matrix, we effectively address the sensitivity issue of existing block sparse learning methods to pre-defined block information, which enables adaptive block estimation while mitigating the risk of overfitting. Based on this, a diversified block sparse Bayesian learning method (**DivSBL**) is proposed, utilizing EM algorithm and dual ascent method for hyperparameter estimation. Moreover, we establish the global and local optimality theory of our model. Experiments validate the advantages of DivSBL over existing algorithms.

Index Terms—Compressed Sensing, Diversified Block Sparse Prior, Sparse Bayesian Learning, Lagrange Dual Ascent.

I. INTRODUCTION

Sparse recovery through Compressive Sensing (CS), with its powerful theoretical foundations and practical utility across various applications, has received much attention [1]. The basic model is considered as

$$\mathbf{y} = \Phi \mathbf{x}, \quad (1)$$

where $\mathbf{y} \in \mathbb{R}^{M \times 1}$ is the measurement (or response) vector and $\Phi \in \mathbb{R}^{M \times N}$ is a known design matrix, satisfying the Unique Representation Property (URP) condition [2], i.e., any of its columns are linearly independent bases. $\mathbf{x} \in \mathbb{R}^{N \times 1}$ ($N \gg M$) is the sparse vector to be recovered. In practice, \mathbf{x} itself is often not sparse but sparse in a certain transformed domain, such as the wavelet domain. Once the signal is compressible in a linear basis Ψ , in other words, $\mathbf{x} = \Psi \mathbf{w}$ where \mathbf{w} exhibits sparsity, and $\Phi \Psi$ satisfies Restricted Isometry Constants (RIP) [3], then we can simply replace \mathbf{x} by $\Psi \mathbf{w}$ in (1) and solve it in the same way. Classic algorithms for compressive sensing and sparse regression include Lasso [4], Sparse Bayesian Learning (SBL) [5], Basis Pursuit (BP) [6], Orthogonal Matching Pursuit (OMP) [7], etc. Recently, there have been approaches that involve solving CS problems through deep learning [8], [9].

However, with the deepening research on compressed sensing and sparse learning, it has been realized that relying solely on the sparsity of \mathbf{x} is insufficient, especially in cases of limited samples [10], [11]. In fact, widely encountered real-world data, such as image and audio, often exhibits clustered sparsity features in transformed domains [12]. The

phenomenon is referred as block sparsity, which means the sparse non-zero entries of \mathbf{x} appear in blocks [10]. Recent years, the study of block sparse model has arisen in machine learning, including adversarial learning [13], image restoration [14], [15], (audio) signal processing [16], [17] and many other areas. Generally, the block structure of \mathbf{x} with g blocks is defined by

$$\mathbf{x} = \underbrace{[x_1 \dots x_{d_1}]}_{\mathbf{x}_1^T} \underbrace{[x_{d_1+1} \dots x_{d_1+d_2}]}_{\mathbf{x}_2^T} \dots \underbrace{[x_{N-d_g+1} \dots x_N]}_{\mathbf{x}_g^T}, \quad (2)$$

where d_i ($i = 1 \dots g$) represent the size of each block and are not necessarily identical. Suppose only k ($k \ll g$) blocks of \mathbf{x} are non-zero, which indicates that \mathbf{x} is block sparse.

Up to now, a number of methods have been proposed to recover block sparse signals. They are mainly divided into two categories.

Block-based: The classical algorithms for processing block sparse scenario include Group-Lasso [18]–[20], Group Basis Pursuit [21], Block-OMP [10] etc. The blocks here are assumed to be static and share a fixed preset block size. Furthermore, Temporally-SBL (TSBL) [22] and Block-SBL (BSBL) [23], [24], based on Bayesian model, provide a more refined estimation of the correlation matrix within blocks. However, it still assumes that elements within the same block simultaneously tend to be either zero or non-zero. Hence, although block-based algorithms can estimate intra-block correlations with high accuracy in block-level recovery, they require a pre-defined choice of suitable block sizes and block patterns, which is too rigid for many practical applications.

Pattern-based: StructOMP [25] is a pattern-based greedy algorithm allowing arbitrary structures, which is a generalization of group sparsity. Another classic algorithm named Pattern-Coupled SBL (PC-SBL) [26], [27], does not have a predefined requirement for block size as well. It utilizes a Bayesian model to couple the signal variances. Building upon PC-SBL, the Burst PC-SBL, proposed in [28], is employed for the estimation of sparse mMIMO channels. While pattern-based algorithms address the issue of explicitly specifying block patterns in block-based algorithms, these models provide a coarse characterization of the intra-block correlation, leading to a loss of structural information within the blocks.

In this paper, we introduce a diversified block sparse Bayesian framework that incorporates diversity in both variance within the same block and intra-block correlation among different blocks. Our model not only inherits the advantages of block-based methods on block-level estimation, but also addresses the longstanding issues associated with such

This work was supported by the National Key R&D Program of China (Grant No. 2021YFA1003300).

Yanhao Zhang, Zhihan Zhu and Yong Xia (corresponding author) are with the School of Mathematical Sciences, Beihang University, Beijing 100191, China. (E-mail: {yanhaozhang, zhihanzhu, yxia}@buaa.edu.cn)

algorithms: the diversified scheme reduces sensitivity to a predefined block size or specified block location, hence accommodates general block sparse data. Based on this model, we develop the DivSBL algorithm, and also analyze both the global minimum and local minima of the constrained cost function (likelihood). The subsequent experiments illustrate the superiority of proposed diversified scheme when applied to real-life block sparse data.

Notation: In this paper, lowercase and uppercase bold symbols will be employed to represent vectors and matrices, respectively. $\det(\mathbf{A})$ denotes the determinant of matrix \mathbf{A} . $\text{tr}(\mathbf{A})$ means the trace of \mathbf{A} . Matrix $\text{diag}(\mathbf{A}_1, \dots, \mathbf{A}_g)$ represents the block diagonal matrix with the matrices $\{\mathbf{A}_i\}_{i=1}^g$ placed along the main diagonal, and $\text{Diag}(\mathbf{A})$ represents the extraction of the diagonal elements from matrix \mathbf{A} to create a vector.

II. A DIVERSIFIED BLOCK SPARSE BAYESIAN MODEL

We consider the block sparse signal recovery, or compressive sensing question in the noisy case

$$\mathbf{y} = \Phi \mathbf{x} + \mathbf{n}, \quad (3)$$

where $\mathbf{n} \sim \mathcal{N}(0, \beta^{-1} \mathbf{I})$ represents the measurement noise. β is a positive precise scalar, and other symbols have the same interpretations as (1). The signal \mathbf{x} exhibits block-sparse structure in (2), but we lack knowledge of the block partition.

Here, for the convenience of algorithm description, we assume that all of the blocks have a equal size L and the full dimension is denoted as $N = gL$. So in the following context, we assume that the signal \mathbf{x} possesses the structure as

$$\mathbf{x} = \underbrace{[x_{11} \dots x_{1L}]_{\mathbf{x}_1^T}}_{\mathbf{x}_1^T} \underbrace{[x_{21} \dots x_{2L}]_{\mathbf{x}_2^T}}_{\mathbf{x}_2^T} \dots \underbrace{[x_{g1} \dots x_{gL}]_{\mathbf{x}_g^T}}_{\mathbf{x}_g^T}^T. \quad (4)$$

In Sections II-A1 and V-B, we will clarify that this assumption is made without loss of generality. In fact, our algorithm can automatically adjust L to an appropriate block size, expanding or contracting as needed.

A. A Diversified Block Sparse Prior

The Diversified Block Sparse prior is proposed in the following scheme. Each block $\mathbf{x}_i \in \mathbb{R}^{L \times 1}$ is assumed to follow a multivariate Gaussian prior

$$p(\mathbf{x}_i; \{\mathbf{G}_i, \mathbf{B}_i\}) = \mathcal{N}(\mathbf{0}, \mathbf{G}_i \mathbf{B}_i \mathbf{G}_i), \quad \forall i = 1, \dots, g, \quad (5)$$

in which, \mathbf{G}_i represents the Diversified Variance matrix, and \mathbf{B}_i represents the Diversified Correlation matrix. The formulation of them are detailed in Sections II-A1 and II-A2. Therefore, the prior distribution of the entire signal \mathbf{x} is denoted as

$$p(\mathbf{x}; \{\mathbf{G}_i, \mathbf{B}_i\}_{i=1}^g) = \mathcal{N}(\mathbf{0}, \Sigma_0), \quad (6)$$

where $\Sigma_0 = \text{diag}\{\mathbf{G}_1 \mathbf{B}_1 \mathbf{G}_1, \mathbf{G}_2 \mathbf{B}_2 \mathbf{G}_2, \dots, \mathbf{G}_g \mathbf{B}_g \mathbf{G}_g\}$. The dependency in this hierarchical model is shown in Figure.1.

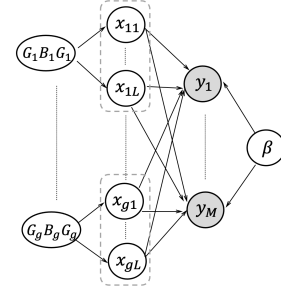


Fig. 1. Directed acyclic graph of diversified block sparse hierarchical structure. The gray nodes represent the response variables, and blank nodes represent the variables to be estimated.

1) *Diversified Variance:* We first execute diversification on variance. In (5), \mathbf{G}_i is defined as

$$\mathbf{G}_i \triangleq \text{diag}\{\sqrt{\gamma_{i1}}, \dots, \sqrt{\gamma_{iL}}\}, \quad (7)$$

and $\mathbf{B}_i \in \mathbb{R}^{L \times L}$ is a positive definite matrix that captures the correlation structure within the i -th block. According to the definition of Pearson correlation, the covariance term $\mathbf{G}_i \mathbf{B}_i \mathbf{G}_i$ in (5) can be specific as

$$\mathbf{G}_i \mathbf{B}_i \mathbf{G}_i = \begin{bmatrix} \gamma_{i1} & \rho_{12}^i \sqrt{\gamma_{i1}} \sqrt{\gamma_{i2}} & \dots & \rho_{1L}^i \sqrt{\gamma_{i1}} \sqrt{\gamma_{iL}} \\ \rho_{21}^i \sqrt{\gamma_{i2}} \sqrt{\gamma_{i1}} & \gamma_{i2} & \dots & \rho_{2L}^i \sqrt{\gamma_{i2}} \sqrt{\gamma_{iL}} \\ \vdots & \vdots & \ddots & \vdots \\ \rho_{L1}^i \sqrt{\gamma_{iL}} \sqrt{\gamma_{i1}} & \rho_{L2}^i \sqrt{\gamma_{iL}} \sqrt{\gamma_{i2}} & \dots & \gamma_{iL} \end{bmatrix},$$

where $\rho_{sk}^i (\forall s, k = 1 \dots L)$ are the elements in correlation matrix \mathbf{B}_i , serving as a visualization of the covariance matrix with displayed structural information.

Now it is evident why assuming equal block sizes L in our model is harmless. For the sake of clarity, we denote the true size of the i -th block \mathbf{x}_i as L_T^i . As illustrated in Figure 2, when $L_T^i < L$, the variances γ_i corresponding to the non-zero positions in \mathbf{x}_i will be learned as non-zero values through posterior inference, while the variances at zero positions will automatically be learned as zero. When $L_T^i > L$, several blocks of the predefined size L covered by the actual block will be updated together, and likewise, variances will be learned as either zero or non-zero. In this way, both of the size and location of the blocks will be automatically learned through posterior inference on the variances.

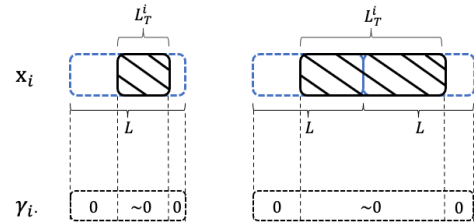


Fig. 2. Left: When $L_T^i < L$. Right: When $L_T^i > L$. The blue dashed line represents the predefined block size and location, and the black shadow represents the actual position of the block with its true size. ' ~ 0 ' denotes non-zero variance.

2) *Diversified Intra-Block Correlation:* Due to the limited data and excessive parameters in intra-block correlation matrices $\mathbf{B}_i (\forall i)$, previous works correct their estimation by imposing strong correlated constraints $\mathbf{B}_i = \mathbf{B}(\forall i)$ to overcome

overfitting [23]. Recognizing that the correlation matrices among different blocks should be diverse but still exhibit some degree of correlation, we choose to apply a weak-correlated constrain to diversify \mathbf{B}_i in the model.

Here we introduce novel weak constraints on \mathbf{B}_i , specifically,

$$\log \det \mathbf{B}_i = \log \det \mathbf{B} \quad \forall i = 1 \dots g, \quad (8)$$

where \mathbf{B} is obtained from the strong constraints $\mathbf{B}_i = \mathbf{B}(\forall i)$ which will be specified in Section III-B. Weak constraints (8) not only capture the distinct correlation structure but also avoid overfitting issue arising from the complete independence among different \mathbf{B}_i .

Furthermore, the constraints imposed here not only maintain the global minimum property of our algorithm, as substantiated in Section IV, but also effectively enhance the convergence rate of the algorithm. There are actually gL^2 constraints in the strong correlated constraints $\mathbf{B}_i = \mathbf{B}(\forall i)$, while with (8), the number of constraints significantly decreases to g , yielding acceleration on the convergence rate. The experimental result is shown below.

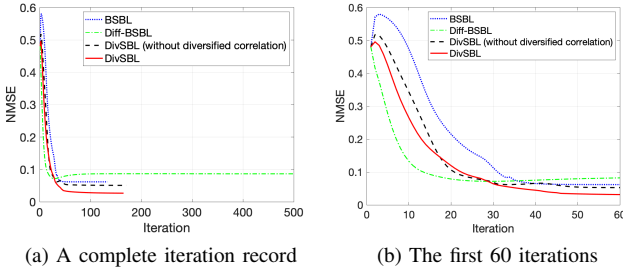


Fig. 3. NMSE with iteration number.

In Figure 3, BSBL adopts strong constraints $\mathbf{B}_i = \mathbf{B}(\forall i)$ on the correlation matrices. With large number of constraints (gL^2) and same correlation matrices, BSBL leads to slow convergence rate and fails to achieve good accuracy. Diff-BSBL imposes no constraints on the correlation matrices, showing faster initial speed but exhibiting overfitting later on. In comparison, DivSBL outperforms DivSBL without diversified intra-block correlation in terms of both speed and accuracy.

In summary, the prior based on (5), (6), (7) and (8) is defined as **diversified block sparse prior**.

3) *Connections to classical models*: Note that the classical Sparse Bayesian Learning models, Relevance Vector Machine (RVM) [5] and Block Sparse Bayesian Learning (BSBL) [22], are special cases of our model.

On the one hand, taking \mathbf{B}_i as identity matrix, diversified block sparse prior (6) immediately degenerates to RVM model

$$p(x_i; \gamma_i) = \mathcal{N}(0, \gamma_i), \quad \forall i = 1, \dots, N, \quad (9)$$

which means ignoring the correlation structure.

On the other hand, when \mathbf{G}_i is scalar matrix $\sqrt{\gamma_i} \mathbf{I}$, the formulation (5) becomes

$$p(\mathbf{x}_i; \{\gamma_i, \mathbf{B}_i\}) = \mathcal{N}(\mathbf{0}, \gamma_i \mathbf{B}_i), \quad \forall i = 1, \dots, g, \quad (10)$$

which is exactly the BSBL model. In this case, all of the elements within a block share a common variance γ_i .

B. Posterior Estimation

By observation model (3), the Gaussian likelihood is

$$p(\mathbf{y} | \mathbf{x}; \beta) = \mathcal{N}(\Phi \mathbf{x}, \beta^{-1} \mathbf{I}). \quad (11)$$

With prior (6) and likelihood (11), the diversified block sparse posterior distribution of \mathbf{x} can be derived based on Bayes' theorem as

$$p(\mathbf{x} | \mathbf{y}; \{\mathbf{G}_i, \mathbf{B}_i\}_{i=1}^g, \beta) = \mathcal{N}(\boldsymbol{\mu}, \boldsymbol{\Sigma}), \quad (12)$$

where

$$\boldsymbol{\mu} = \beta \boldsymbol{\Sigma} \Phi^T \mathbf{y}, \quad (13)$$

$$\boldsymbol{\Sigma} = \left(\boldsymbol{\Sigma}_0^{-1} + \beta \Phi^T \Phi \right)^{-1}. \quad (14)$$

After estimating all hyperparameters in (12), i.e., $\hat{\Theta} = \{\{\hat{\mathbf{G}}_i\}_{i=1}^g, \{\hat{\mathbf{B}}_i\}_{i=1}^g, \hat{\beta}\}$, as described in Section III, the Maximum A Posterior (MAP) estimation of \mathbf{x} is formulated as

$$\hat{\mathbf{x}}^{MAP} = \hat{\boldsymbol{\mu}}. \quad (15)$$

III. BAYESIAN INFERENCE: DIVSBL ALGORITHM

A. EM Formulation

To estimate $\Theta = \{\{\mathbf{G}_i\}_{i=1}^g, \{\mathbf{B}_i\}_{i=1}^g, \beta\}$, either Type-II Maximum Likelihood [29] or Expectation-Maximization (EM) formulation [30] can be employed.

Following the EM procedure, our goal is to maximize $p(\mathbf{y}; \Theta)$, or equivalently $\log p(\mathbf{y}; \Theta)$. Defining this objective function as $\mathcal{L}(\Theta)$, the problem can be expressed as

$$\max_{\Theta} \mathcal{L}(\Theta) = -\mathbf{y}^T \boldsymbol{\Sigma}_y^{-1} \mathbf{y} - \log \det \boldsymbol{\Sigma}_y, \quad (16)$$

where $\boldsymbol{\Sigma}_y = \beta^{-1} \mathbf{I} + \Phi \boldsymbol{\Sigma}_0 \Phi^T$. Then, treating \mathbf{x} as a hidden variable in E-step, we have the Q function as

$$\begin{aligned} Q(\Theta) &= E_{\mathbf{x} | \mathbf{y}; \Theta^{t-1}} [\log p(\mathbf{y}, \mathbf{x}; \Theta)] \\ &= E_{\mathbf{x} | \mathbf{y}; \Theta^{t-1}} [\log p(\mathbf{y} | \mathbf{x}; \beta)] \\ &\quad + E_{\mathbf{x} | \mathbf{y}; \Theta^{t-1}} [\log p(\mathbf{x}; \{\mathbf{G}_i\}_{i=1}^g, \{\mathbf{B}_i\}_{i=1}^g)] \\ &\triangleq Q(\beta) + Q(\{\mathbf{G}_i\}_{i=1}^g, \{\mathbf{B}_i\}_{i=1}^g), \end{aligned} \quad (17)$$

where Θ^{t-1} denotes the parameter estimated in the latest iteration. As indicated in (17), we have divided Q function into two parts: $Q(\beta) \triangleq E_{\mathbf{x} | \mathbf{y}; \Theta^{t-1}} [\log p(\mathbf{y} | \mathbf{x}; \beta)]$ depends solely on β , and $Q(\{\mathbf{G}_i\}_{i=1}^g, \{\mathbf{B}_i\}_{i=1}^g) \triangleq E_{\mathbf{x} | \mathbf{y}; \Theta^{t-1}} [\log p(\mathbf{x}; \{\mathbf{G}_i\}_{i=1}^g, \{\mathbf{B}_i\}_{i=1}^g)]$ only on $\{\mathbf{G}_i\}_{i=1}^g$ and $\{\mathbf{B}_i\}_{i=1}^g$. Therefore, the parameters of these two Q functions can be updated separately.

In M-step, we need to maximize the above Q functions to obtain the estimation of Θ . We observe that

$$\begin{aligned} Q(\{\mathbf{G}_i\}_{i=1}^g, \{\mathbf{B}_i\}_{i=1}^g) &\propto -\frac{1}{2} E_{\mathbf{x} | \mathbf{y}; \Theta^{t-1}} (\log |\boldsymbol{\Sigma}_0| + \mathbf{x}^T \boldsymbol{\Sigma}_0 \mathbf{x}) \\ &= -\frac{1}{2} \log |\boldsymbol{\Sigma}_0| - \frac{1}{2} \text{tr} [\boldsymbol{\Sigma}_0^{-1} (\boldsymbol{\Sigma} + \boldsymbol{\mu} \boldsymbol{\mu}^T)], \end{aligned} \quad (18)$$

in which Σ_0 can be reformulated as

$$\begin{aligned}\Sigma_0 &= \text{diag} \{ \mathbf{G}_1 \mathbf{B}_1 \mathbf{G}_1, \dots, \mathbf{G}_g \mathbf{B}_g \mathbf{G}_g \} \\ &= \mathbf{D}_{-i} + \begin{pmatrix} \mathbf{0} \\ \mathbf{I}_L \\ \mathbf{0} \end{pmatrix} \mathbf{G}_i \mathbf{B}_i \mathbf{G}_i \begin{pmatrix} \mathbf{0} & \mathbf{I}_L & \mathbf{0} \end{pmatrix} \\ &= \mathbf{D}_{-i} + \begin{pmatrix} \mathbf{0} \\ \mathbf{I}_L \\ \mathbf{0} \end{pmatrix} (\sqrt{\gamma_{ij}} \mathbf{P}_j + \mathbf{W}_{-j}^i) \mathbf{B}_i \\ &\quad \times (\sqrt{\gamma_{ij}} \mathbf{P}_j + \mathbf{W}_{-j}^i) \begin{pmatrix} \mathbf{0} & \mathbf{I}_L & \mathbf{0} \end{pmatrix},\end{aligned}\quad (19)$$

where

$$\mathbf{D}_{-i} = \text{diag} \left\{ \mathbf{G}_1 \mathbf{B}_1 \mathbf{G}_1, \dots, \mathbf{G}_{i-1} \mathbf{B}_{i-1} \mathbf{G}_{i-1}, \right. \\ \left. \mathbf{0}_{L \times L}, \mathbf{G}_{i+1} \mathbf{B}_{i+1} \mathbf{G}_{i+1}, \dots, \mathbf{G}_g \mathbf{B}_g \mathbf{G}_g \right\},$$

$$\mathbf{P}_j = \text{diag} \{ \delta_{1j}, \delta_{2j}, \dots, \delta_{Lj} \},$$

$$\mathbf{W}_{-j}^i = \text{diag} \{ \sqrt{\gamma_{i1}}, \dots, \sqrt{\gamma_{i,j-1}}, 0, \sqrt{\gamma_{i,j+1}}, \dots, \sqrt{\gamma_{iL}} \},$$

and the Kronecker delta function here, denoted by δ_{ij} , is defined as

$$\delta_{ij} = \begin{cases} 1, & \text{if } i = j, \\ 0, & \text{otherwise.} \end{cases}$$

Hence, Σ_0 is split into two components in (19), with the second term of the summation only depending on \mathbf{G}_i and \mathbf{B}_i , and the first part \mathbf{D}_{-i} being entirely unrelated to them. Then, we can update each \mathbf{B}_i and \mathbf{G}_i independently, allowing us to learn diverse \mathbf{B}_i and \mathbf{G}_i for different blocks.

The gradient of (18) with respect to $\sqrt{\gamma_{ij}}$ can be expressed as

$$\begin{aligned}\frac{\partial Q(\{\mathbf{G}_i\}_{i=1}^g, \{\mathbf{B}_i\}_{i=1}^g)}{\partial \sqrt{\gamma_{ij}}} &= \frac{\partial(-\frac{1}{2} \log |\Sigma_0|)}{\partial \sqrt{\gamma_{ij}}} \\ &\quad + \frac{\partial(-\frac{1}{2} \text{tr} [\Sigma_0^{-1}(\Sigma + \mu \mu^T)])}{\partial \sqrt{\gamma_{ij}}}.\end{aligned}$$

The first term results in

$$\frac{\partial(-\frac{1}{2} \log |\Sigma_0|)}{\partial \sqrt{\gamma_{ij}}} = -\text{tr} (\mathbf{P}_j (\mathbf{G}_i \mathbf{B}_i \mathbf{G}_i)^{-1} \mathbf{G}_i \mathbf{B}_i) = -\frac{1}{\sqrt{\gamma_{ij}}},$$

and the second term yields

$$\begin{aligned}\frac{\partial(-\frac{1}{2} \text{tr} [\Sigma_0^{-1}(\Sigma + \mu \mu^T)])}{\partial \sqrt{\gamma_{ij}}} &= \text{tr} [\mathbf{P}_j (\mathbf{G}_i \mathbf{B}_i \mathbf{G}_i)^{-1} (\Sigma^i + \mu^i (\mu^i)^T) \mathbf{G}_i^{-1}] \\ &= \text{tr} [\mathbf{B}_i^{-1} \mathbf{G}_i^{-1} (\Sigma^i + \mu^i (\mu^i)^T) \mathbf{P}_j \gamma_{ij}^{-1}].\end{aligned}$$

where $\mu^i \in \mathbb{R}^{L \times 1}$ represents the i -th block in μ , and $\Sigma^i \in \mathbb{R}^{L \times L}$ denotes the i -th block in Σ ¹. Using $\mathbf{A}_1(\mathbf{M} +$

¹Using MATLAB notation, $\mu^i \triangleq \mu((i-1)L+1:iL)$, $\Sigma^i \triangleq \Sigma((i-1)L+1:iL, (i-1)L+1:iL)$.

$\mathbf{N})\mathbf{A}_2 = \mathbf{A}_1 \mathbf{M} \mathbf{A}_2 + \mathbf{A}_1 \mathbf{N} \mathbf{A}_2$, the formula above can be further transformed into

$$\begin{aligned}&\frac{\partial(-\frac{1}{2} \text{tr} [\Sigma_0^{-1}(\Sigma + \mu \mu^T)])}{\partial \sqrt{\gamma_{ij}}} \\ &= \text{tr} \left[\mathbf{B}_i^{-1} \frac{1}{\sqrt{\gamma_{ij}}} \mathbf{P}_j (\Sigma^i + \mu^i (\mu^i)^T) \mathbf{P}_j \gamma_{ij}^{-1} \right] \\ &\quad + \text{tr} [\mathbf{B}_i^{-1} (\mathbf{I} - \mathbf{P}_j) \mathbf{G}_i^{-1} (\Sigma^i + \mu^i (\mu^i)^T) \mathbf{P}_j \gamma_{ij}^{-1}] \\ &= \left(\frac{1}{\sqrt{\gamma_{ij}}} \right)^3 \mathbf{A}_{ij} + \frac{1}{\gamma_{ij}} \mathbf{T}_{ij},\end{aligned}$$

in which, \mathbf{T}_{ij} and \mathbf{A}_{ij} are independent of $\sqrt{\gamma_{ij}}$, and their expressions are

$$\begin{aligned}\mathbf{T}_{ij} &= [(\mathbf{B}_i^{-1})_j \odot \text{diag}(\mathbf{W}_{-j}^i)^{-1}] \cdot (\Sigma^i + \mu^i (\mu^i)^T)_{,j}, \\ \mathbf{A}_{ij} &= (\mathbf{B}_i^{-1})_{jj} \cdot \left(\Sigma^i + \mu^i (\mu^i)^T \right)_{jj}.\end{aligned}$$

Thus, the derivative of $Q(\Theta)$ with respect to $\sqrt{\gamma_{ij}}$ reads as

$$\frac{\partial Q(\Theta)}{\partial \sqrt{\gamma_{ij}}} = -\frac{1}{\sqrt{\gamma_{ij}}} + \left(\frac{1}{\sqrt{\gamma_{ij}}} \right)^3 \mathbf{A}_{ij} + \frac{1}{\gamma_{ij}} \mathbf{T}_{ij}. \quad (20)$$

It is important to note that the variance should be non-negative. So by setting (20) equal to zero, we obtain the update formulation of γ_{ij} as

$$\gamma_{ij} = \frac{4\mathbf{A}_{ij}^2}{(\sqrt{\mathbf{T}_{ij}^2 + 4\mathbf{A}_{ij}} - \mathbf{T}_{ij})^2}. \quad (21)$$

As for the gradient of (18) with respect to \mathbf{B}_i , we have

$$\begin{aligned}&\frac{\partial Q(\{\mathbf{G}_i\}_{i=1}^g, \{\mathbf{B}_i\}_{i=1}^g)}{\partial \mathbf{B}_i} \\ &= -\frac{1}{2} \mathbf{B}_i^{-1} + \frac{1}{2} \mathbf{B}_i^{-1} \mathbf{G}_i^{-1} (\Sigma^i + \mu^i (\mu^i)^T) \mathbf{G}_i^{-1} \mathbf{B}_i^{-1}.\end{aligned}$$

Setting it equal to zero, the learning rule for \mathbf{B}_i is given by

$$\mathbf{B}_i = \mathbf{G}_i^{-1} \left(\Sigma^i + \mu^i (\mu^i)^T \right) \mathbf{G}_i^{-1}. \quad (22)$$

The update formula of β is derived in the same way as [22]. The learning rule is given by

$$\beta = \frac{M}{\|\mathbf{y} - \Phi \mu\|_2^2 + \text{tr} (\Sigma \Phi^T \Phi)}. \quad (23)$$

B. Diversified Correlation Matrices by Dual Ascent

In this subsection, we propose the algorithm for solving the correlation matrix estimation problem satisfying (8). As mentioned in Section II-A2, previous studies have employed strong constraints $\mathbf{B}_i = \mathbf{B}(\forall i)$, i.e.,

$$\mathbf{B} = \mathbf{B}_i = \frac{1}{g} \sum_{i=1}^g \mathbf{G}_i^{-1} \left(\Sigma^i + \mu^i (\mu^i)^T \right) \mathbf{G}_i^{-1}. \quad (24)$$

In diversified scheme, we apply weak-correlated constraints (8) to diversify \mathbf{B}_i . Therefore, the problem of maximizing the Q function with respect to \mathbf{B}_i becomes

$$\begin{aligned}\max_{\mathbf{B}_i} & Q(\{\mathbf{B}_i\}_{i=1}^g, \{\mathbf{G}_i\}_{i=1}^g) \\ \text{s. t.} & \log \det \mathbf{B}_i = \log \det \mathbf{B} \quad \forall i = 1 \dots g,\end{aligned}\quad (25)$$

which is equivalent to (in the sense that both share the same optimal solution)

$$\begin{aligned} \min_{\mathbf{B}_i} \quad & \frac{1}{2} \log \det \boldsymbol{\Sigma}_0 + \frac{1}{2} \text{tr} [\boldsymbol{\Sigma}_0^{-1} (\boldsymbol{\Sigma} + \boldsymbol{\mu} \boldsymbol{\mu}^T)] \\ \text{s. t.} \quad & \log \det \mathbf{B}_i = \log \det \mathbf{B} \quad \forall i = 1 \dots g, \end{aligned} \quad (\text{P})$$

where \mathbf{B} is already derived in (24). Therefore, by solving (P), we will obtain diversified solution for the correlation matrices $\mathbf{B}_i, \forall i$.

An efficient way to handle this constrained optimization is to solve its dual problem. In general, the dual problem is a lower bound of its primal objective. There are many possible choices of dual problem, but most refers to the Lagrange dual [31]. We consider focusing on (P)'s Lagrange dual problem to solve the constrained optimization problem here.

To clarify the dual problem of (P), we firstly express (P)'s Lagrange function as

$$\begin{aligned} \mathcal{L}(\{\mathbf{B}_i\}_{i=1}^g; \{\lambda_i\}_{i=1}^g) = & \frac{1}{2} \log \det \boldsymbol{\Sigma}_0 + \frac{1}{2} \text{tr} [\boldsymbol{\Sigma}_0^{-1} (\boldsymbol{\Sigma} + \boldsymbol{\mu} \boldsymbol{\mu}^T)] \\ & + \sum_{i=1}^g \lambda_i (\log \det \mathbf{B}_i - \log \det \mathbf{B}). \end{aligned} \quad (26)$$

Since the constraints in (P) are equalities, we do not impose any requirements on the multipliers $\{\lambda_i\}_{i=1}^g$. The primal and dual problems in terms of \mathcal{L} are given by

$$\min_{\{\mathbf{B}_i\}_{i=1}^g} \max_{\{\lambda_i\}_{i=1}^g} \mathcal{L}(\{\mathbf{B}_i\}_{i=1}^g; \{\lambda_i\}_{i=1}^g), \quad (\text{P})$$

$$\max_{\{\lambda_i\}_{i=1}^g} \min_{\{\mathbf{B}_i\}_{i=1}^g} \mathcal{L}(\{\mathbf{B}_i\}_{i=1}^g; \{\lambda_i\}_{i=1}^g), \quad (\text{D})$$

respectively. Although the objection here is non-convex, dual ascent method takes advantage of the fact that the dual problem is always convex [31], and we can get a lower bound of (P) by solving (D). Specifically, dual ascent method employs gradient ascent on the dual variables. As long as the step sizes are chosen properly, the algorithm would converge to a local maximum. We will demonstrate how to choose the step sizes in the following paragraph.

According to this framework, we first solve the inner minimization problem of the dual problem (D). Keeping the multipliers $\{\lambda_i\}_{i=1}^g$ fixed, the inner problem is

$$\begin{aligned} \mathbf{B}_i^{k+1} \in \arg \min_{\mathbf{B}_i} \mathcal{L}(\{\mathbf{B}_i\}_{i=1}^g; \{\lambda_i\}_{i=1}^g) \\ = \arg \min_{\mathbf{B}_i} \mathcal{L}(\mathbf{B}_i; \lambda_i^k), \end{aligned} \quad (27)$$

where the superscript k implies the k -th iteration. According to the first-order optimality condition, the primal solution for (27) is as follows:

$$\mathbf{B}_i^{k+1} = \frac{\mathbf{G}_i^{-1} (\boldsymbol{\Sigma}^i + \boldsymbol{\mu}^i (\boldsymbol{\mu}^i)^T) \mathbf{G}_i^{-1}}{1 + 2\lambda_i^k}. \quad (28)$$

Subsequently, the outer maximization problem for the multiplier λ_i (dual variable) can be addressed using the gradient ascent method. The update formulation is obtained by

$$\begin{aligned} \lambda_i^{k+1} &= \lambda_i^k + \alpha_i^k \nabla_{\lambda_i} \mathcal{L}(\{\mathbf{B}_i^k\}_{i=1}^g; \{\lambda_i\}_{i=1}^g) \\ &= \lambda_i^k + \alpha_i^k \nabla_{\lambda_i} \mathcal{L}(\mathbf{B}_i^k; \lambda_i) \\ &= \lambda_i^k + \alpha_i^k (\log \det \mathbf{B}_i^k - \log \det \mathbf{B}), \end{aligned} \quad (29)$$

in which, α_i^k represents the step size in the k -th iteration for updating the multiplier λ_i ($i = 1 \dots g$). Convergence is only guaranteed if the step size satisfies $\sum_{k=1}^{\infty} \alpha_i^k = \infty$ and $\sum_{k=1}^{\infty} (\alpha_i^k)^2 < \infty$ [31]. Therefore, we choose a diminishing step size $1/k$ to ensure the convergence. The procedure, using dual ascent method to diversify \mathbf{B}_i , is summarized in Algorithm 1 as follows:

Algorithm 1 Diversifying \mathbf{B}_i

- 1: **Input:** Initialized $\lambda_i^0 \in \mathbf{R}, \varepsilon > 0$, the common intra-block correlation \mathbf{B} obtained from (24).
 - 2: **Output:** $\mathbf{B}_i, i = 1, \dots, g$.
 - 3: Set iteration count $k = 1$.
 - 4: **repeat**
 - 5: Set step size $\alpha_i^k = 1/k$.
 - 6: Update \mathbf{B}_i^{k+1} using (28).
 - 7: Update λ_i^{k+1} using (29)
 - 8: $k := k + 1$;
 - 9: **until** $|\log \det \mathbf{B}_i^k - \log \det \mathbf{B}| \leq \varepsilon$.
-

Since our objective is to maximize the likelihood function (16), and solving sub-problem (P) is aimed at generating a convergent sequence, it is unnecessary to solve the sub-problem precisely. In practice, only a single iteration in dual ascent is sufficient, yielding satisfactory precision and significant time savings in experiment. Actually, we merely impose hidden unknown weak constraints, which may be weaker than the explicit $\log \det(\cdot)$ and correspond to the optimal solution of a certain Lagrange function. Even if the explicit $\log \det(\cdot)$ constraint model is solved accurately, the optimal solution cannot be provided.

Considering that it's sufficient to model elements of a block as a first order Auto-Regression (AR) process [23] in which the intra-block correlation matrix is a Toeplitz matrix, we employ this strategy for \mathbf{B}_i . After estimating \mathbf{B}_i by dual ascent, we then apply Toeplitz correction to \mathbf{B}_i as

$$\begin{aligned} \mathbf{B}_i &= \text{Toeplitz}([1, r, \dots, r^{L-1}]) \\ &= \begin{bmatrix} 1 & r & \dots & r^{L-1} \\ \vdots & \vdots & \ddots & \vdots \\ r^{L-1} & r^{L-2} & \dots & 1 \end{bmatrix}, \end{aligned} \quad (30)$$

where $r \triangleq \frac{m_1}{m_0}$ is the approximate AR coefficient, m_0 represents the average of elements along the main diagonal of \mathbf{B}_i , and m_1 represents the average of elements along the main sub-diagonal of \mathbf{B}_i .

In conclusion, the Diversified SBL (**DivSBL**) algorithm is summarized as Algorithm 2 presented below.

IV. GLOBAL MINIMUM AND LOCAL MINIMA

For the sake of simplicity, we denote the true signal as \mathbf{x}_{true} , which is the sparsest among all feasible solutions. The block sparsity of the true signal is denoted as K_0 , indicating the presence of K_0 blocks. Let $\tilde{\mathbf{G}} \triangleq \text{diag}(\sqrt{\gamma_{11}}, \dots, \sqrt{\gamma_{gL}})$, $\tilde{\mathbf{B}} \triangleq \text{diag}(\mathbf{B}_1, \dots, \mathbf{B}_g)$, thus $\boldsymbol{\Sigma}_0 = \tilde{\mathbf{G}} \tilde{\mathbf{B}} \tilde{\mathbf{G}}$. Additionally,

²The index i here exclude those indices already removed in the 5th line of the algorithm.

Algorithm 2 DivSBL Algorithm

1: **Input:** Φ, \mathbf{y} , initialized $\gamma \in \mathbb{R}^n, \Sigma_0, \beta > 0, \lambda^0$.
 2: **Output:** $\hat{\mathbf{x}}^{MAP}, \hat{\Sigma}, \hat{\gamma}, \hat{\mathbf{B}}_i, \hat{\beta}$.
 3: **repeat**
 4: **if** $\text{mean}(\gamma_{l_i}) < \text{threshold}$ **then**
 5: Prune γ_{l_i} from the model (set $\gamma_{l_i} = \mathbf{0}$).
 6: Set the corresponding $\mu^l = \mathbf{0}, \Sigma^l = \mathbf{0}_{L \times L}$.
 7: **end if**
 8: Update γ_{ij} by (21)².
 9: Update \mathbf{B} by (24).
 10: Update \mathbf{B}_i, λ_i by (28)(29).
 11: Execute Toeplitz correction for \mathbf{B}_i using (30).
 12: Update μ and Σ by (13)(14).
 13: Update β using (23).
 14: **until** convergence criterion met
 15: $\hat{\mathbf{x}}^{MAP} = \mu$.

we assume that the measurement matrix Φ satisfies the URP condition [2].

Because our model can degrade to BSBL [22] and RVM [32] models, some of the proof strategies here are modeled after them. However, it is important to note that, due to the highly non-linear structure of variance γ in diversified block sparse prior (5), the proof here has become significantly more challenging, particularly in the analysis of local minima. We employed various techniques in the proof, such as Schur complement and vectorization, resulting in improved conclusions.

A. Analysis of Global Minimum

By introducing a negative sign to the cost function (16), we have the following result on the property of global minimum and the phase transition for block sparsity K_0 .

Theorem 1. *As $\beta \rightarrow \infty$ (noiseless) and $K_0 < (M + 1)/2L$, the unique global minimum $\hat{\gamma} \triangleq (\hat{\gamma}_{11}, \dots, \hat{\gamma}_{gL})^T$ yields a recovery $\hat{\mathbf{x}}$ by (13) that is equal to \mathbf{x}_{true} , regardless of the estimated $\hat{\mathbf{B}}_i$ ($\forall i$).*

The proof draws inspiration from [32] and is provided in detail in Appendix A.

Theorem 1 illustrates that, under noiseless conditions, when block sparsity of the true signal satisfies the aforementioned upper bound, attaining the global minimum of variance enables the exact recovery of the true signal. As this result is independent of $\hat{\mathbf{B}}_i$, the diversified constraints on $\hat{\mathbf{B}}_i$ do not affect the convergence result.

B. Analysis of Local Minima

Before presenting the theory for local minima, we provide two lemmas firstly.

Lemma 1. *For any semi-definite positive symmetric matrix $\mathbf{Z} \in \mathbb{R}^{M \times M}$, the constraint $\mathbf{Z} \succeq \Phi \Sigma_0 \Phi^T$ is convex with respect to \mathbf{Z} and γ .*

Proof. According to the Schur complement [31], $\mathbf{Z} \succeq \Phi \Sigma_0 \Phi^T$ is equivalent to

$$\begin{pmatrix} \mathbf{Z} & \Phi \\ \Phi^T & \Sigma_0^{-1} \end{pmatrix} \succeq \mathbf{0}. \quad (31)$$

Introducing a new symmetric matrix $\mathbf{Y} \in \mathbb{R}^{N \times N}$ here, (31) can be formulated equivalently as

$$\begin{cases} \begin{pmatrix} \mathbf{Z} & \Phi \\ \Phi^T & \mathbf{Y} \end{pmatrix} \succeq \mathbf{0} \\ \Sigma_0^{-1} \preceq \mathbf{Y} \end{cases}. \quad (32)$$

We can see that the first semi-definite positive constraint in (32) is convex with respect to \mathbf{Z} and \mathbf{Y} , so we only need to illustrate the convexity of the second constraint.

Take $\forall \xi, \eta \succeq 0$, which satisfy $\Sigma_0^{-1}(\xi) - \mathbf{Y}_1 \preceq 0$ and $\Sigma_0^{-1}(\eta) - \mathbf{Y}_2 \preceq 0$, i.e.,

$$\begin{pmatrix} \frac{1}{\sqrt{\xi_{11}}} & & \\ & \ddots & \\ & & \frac{1}{\sqrt{\xi_{gL}}} \end{pmatrix} \tilde{\mathbf{B}}^{-1} \begin{pmatrix} \frac{1}{\sqrt{\xi_{11}}} & & \\ & \ddots & \\ & & \frac{1}{\sqrt{\xi_{gL}}} \end{pmatrix} - \mathbf{Y}_1 \preceq 0,$$

$$\begin{pmatrix} \frac{1}{\sqrt{\eta_{11}}} & & \\ & \ddots & \\ & & \frac{1}{\sqrt{\eta_{gL}}} \end{pmatrix} \tilde{\mathbf{B}}^{-1} \begin{pmatrix} \frac{1}{\sqrt{\eta_{11}}} & & \\ & \ddots & \\ & & \frac{1}{\sqrt{\eta_{gL}}} \end{pmatrix} - \mathbf{Y}_2 \preceq 0.$$

For convenience, denote

$$\mathbf{D}_1 = \begin{pmatrix} \frac{1}{\sqrt{\xi_{11}}} & & \\ & \ddots & \\ & & \frac{1}{\sqrt{\xi_{gL}}} \end{pmatrix}, \mathbf{D}_2 = \begin{pmatrix} \frac{1}{\sqrt{\eta_{11}}} & & \\ & \ddots & \\ & & \frac{1}{\sqrt{\eta_{gL}}} \end{pmatrix},$$

$$\mathbf{D}_3 = \begin{pmatrix} \frac{1}{\sqrt{(1-\alpha)\xi_{11} + \alpha\eta_{11}}} & & \\ & \ddots & \\ & & \frac{1}{\sqrt{(1-\alpha)\xi_{gL} + \alpha\eta_{gL}}} \end{pmatrix},$$

where $\alpha \in [0, 1]$. Since $\frac{1}{\sqrt{\xi_{ij}}}$ is convex, we have

$$\frac{1}{\sqrt{(1-\alpha)\xi_{ij} + \alpha\eta_{ij}}} \leq \frac{1-\alpha}{\sqrt{\xi_{ij}}} + \frac{\alpha}{\sqrt{\eta_{ij}}}.$$

Then the convex combination of the variables can be relaxed as

$$\mathbf{D}_3 \tilde{\mathbf{B}}^{-1} \mathbf{D}_3 \preceq [(1-\alpha)\mathbf{D}_1 + \alpha\mathbf{D}_2] \tilde{\mathbf{B}}^{-1} [(1-\alpha)\mathbf{D}_1 + \alpha\mathbf{D}_2]. \quad (33)$$

Transform the right-hand side of (33) into a scalar by multiplying any vector \mathbf{z} , i.e.,

$$\begin{aligned} & \mathbf{z}^T [(1-\alpha)\mathbf{D}_1 + \alpha\mathbf{D}_2] \tilde{\mathbf{B}}^{-1} [(1-\alpha)\mathbf{D}_1 + \alpha\mathbf{D}_2] \mathbf{z} \\ &= \text{Diag}([(1-\alpha)\mathbf{D}_1 + \alpha\mathbf{D}_2])^T \text{diag}(\mathbf{z}) \tilde{\mathbf{B}}^{-1} \\ & \quad \cdot \text{diag}(\mathbf{z}) \text{Diag}([(1-\alpha)\mathbf{D}_1 + \alpha\mathbf{D}_2]) \\ & \triangleq \text{Diag}([(1-\alpha)\mathbf{D}_1 + \alpha\mathbf{D}_2])^T \mathbf{Q} \text{Diag}([(1-\alpha)\mathbf{D}_1 + \alpha\mathbf{D}_2]) \\ & \leq (1-\alpha) \text{Diag}(\mathbf{D}_1)^T \mathbf{Q} \text{Diag}(\mathbf{D}_1) + \alpha \text{Diag}(\mathbf{D}_2)^T \mathbf{Q} \text{Diag}(\mathbf{D}_2), \end{aligned} \quad (34)$$

in which we denote $\mathbf{Q} = \text{diag}(\mathbf{z}) \tilde{\mathbf{B}}^{-1} \text{diag}(\mathbf{z})$, and the last inequality is from the Jensen's inequality.

Therefore, using the result that matrix $\mathbf{A}_1 \preceq \mathbf{A}_2 \Leftrightarrow \mathbf{z}^T \mathbf{A}_1 \mathbf{z} \leq \mathbf{z}^T \mathbf{A}_2 \mathbf{z} (\forall \mathbf{z})$, (34) results in

$$[(1-\alpha)\mathbf{D}_1 + \alpha\mathbf{D}_2] \tilde{\mathbf{B}}^{-1} [(1-\alpha)\mathbf{D}_1 + \alpha\mathbf{D}_2] \quad (35)$$

$$\preceq (1-\alpha)\mathbf{D}_1 \tilde{\mathbf{B}}^{-1} \mathbf{D}_1 + \alpha\mathbf{D}_2 \tilde{\mathbf{B}}^{-1} \mathbf{D}_2. \quad (36)$$

According to (33) and (36), we have

$$\begin{aligned} & \mathbf{D}_3 \tilde{\mathbf{B}}^{-1} \mathbf{D}_3 - [(1 - \alpha) \mathbf{Y}_1 + \alpha \mathbf{Y}_2] \\ & \preceq (1 - \alpha) [\mathbf{D}_1 \tilde{\mathbf{B}}^{-1} \mathbf{D}_1 - \mathbf{Y}_1] + \alpha [\mathbf{D}_2 \tilde{\mathbf{B}}^{-1} \mathbf{D}_2 - \mathbf{Y}_2] \preceq \mathbf{0}, \end{aligned}$$

which indicates that

$$\Sigma_0^{-1} ((1 - \alpha) \boldsymbol{\xi} + \alpha \boldsymbol{\eta}) - [(1 - \alpha) \mathbf{Y}_1 + \alpha \mathbf{Y}_2] \preceq \mathbf{0}.$$

Hence, (31) is convex with respect to \mathbf{Z} and $\boldsymbol{\gamma}$, which concludes the proof. \square

Lemma 2. $\mathbf{y}^T \Sigma_y^{-1} \mathbf{y} = C \Leftrightarrow \mathbf{P}(\sqrt{\boldsymbol{\gamma}} \otimes \sqrt{\boldsymbol{\gamma}}) = \mathbf{b}$ for any constant C , where $\mathbf{b} \triangleq \mathbf{y} - \beta^{-1} \mathbf{u}$, $\mathbf{P} \triangleq [(\mathbf{u}^T \boldsymbol{\Phi}) \otimes \boldsymbol{\Phi}] \text{diag}(\text{vec}(\tilde{\mathbf{B}}))$, and \mathbf{u} is a vector satisfying $\mathbf{y}^T \mathbf{u} = C$.

Proof. " \Rightarrow " Given $\mathbf{y}^T \Sigma_y^{-1} \mathbf{y} = C$ and \mathbf{u} satisfying $\mathbf{y}^T \mathbf{u} = C$, without loss of generality, we choose $\mathbf{u} \triangleq \Sigma_y^{-1} \mathbf{y}$, i.e., $\mathbf{y} = \Sigma_y \mathbf{u}$. Then \mathbf{b} can be rewritten as

$$\mathbf{b} = (\Sigma_y - \beta^{-1} \mathbf{I}) \mathbf{u} = \boldsymbol{\Phi} \Sigma_0 \boldsymbol{\Phi}^T \mathbf{u}. \quad (37)$$

Applying the vectorization operation to both sides of the equation, (37) results in

$$\begin{aligned} \mathbf{b} &= \text{vec}(\boldsymbol{\Phi} \Sigma_0 \boldsymbol{\Phi}^T \mathbf{u}) \\ &= [(\mathbf{u}^T \boldsymbol{\Phi}) \otimes \boldsymbol{\Phi}] \text{vec}(\Sigma_0) \\ &= [(\mathbf{u}^T \boldsymbol{\Phi}) \otimes \boldsymbol{\Phi}] \text{vec}(\tilde{\mathbf{G}} \tilde{\mathbf{B}} \tilde{\mathbf{G}}) \\ &= [(\mathbf{u}^T \boldsymbol{\Phi}) \otimes \boldsymbol{\Phi}] (\tilde{\mathbf{G}} \otimes \tilde{\mathbf{G}}) \text{vec}(\tilde{\mathbf{B}}) \\ &= [(\mathbf{u}^T \boldsymbol{\Phi}) \otimes \boldsymbol{\Phi}] \text{diag}(\text{vec}(\tilde{\mathbf{B}})) \text{Diag}(\tilde{\mathbf{G}} \otimes \tilde{\mathbf{G}}) \\ &= [(\mathbf{u}^T \boldsymbol{\Phi}) \otimes \boldsymbol{\Phi}] \text{diag}(\text{vec}(\tilde{\mathbf{B}})) \cdot (\sqrt{\boldsymbol{\gamma}} \otimes \sqrt{\boldsymbol{\gamma}}). \end{aligned}$$

" \Leftarrow " Vice versa. \square

It's clear that \mathbf{P} is a full row rank matrix, i.e., $r(\mathbf{P}) = M$. Given the above lemmas, we arrive at the following result.

Theorem 2. When $\beta \rightarrow \infty$ (noiseless), every local minimum of the cost function (16) with respect to $\boldsymbol{\gamma}$ satisfies $\|\hat{\boldsymbol{\gamma}}\|_0 \leq \sqrt{M}$, irrespective of the estimated $\hat{\mathbf{B}}_i$ ($\forall i$).

Proof. Consider the following optimization problem,

$$\begin{aligned} \min_{\boldsymbol{\gamma}} \quad & \log \det \Sigma_y \\ \text{s. t.} \quad & \mathbf{P}(\sqrt{\boldsymbol{\gamma}} \otimes \sqrt{\boldsymbol{\gamma}}) = \mathbf{b} \\ & \boldsymbol{\gamma} \succeq \mathbf{0}, \end{aligned} \quad (38)$$

where $\Sigma_y = \beta^{-1} \mathbf{I} + \boldsymbol{\Phi} \Sigma_0 \boldsymbol{\Phi}^T$. So when $\beta \rightarrow \infty$, (38) becomes

$$\begin{aligned} \min_{\boldsymbol{\gamma}} \quad & \log \det(\boldsymbol{\Phi} \Sigma_0 \boldsymbol{\Phi}^T) \\ \text{s. t.} \quad & \mathbf{P}(\sqrt{\boldsymbol{\gamma}} \otimes \sqrt{\boldsymbol{\gamma}}) = \mathbf{b} \\ & \boldsymbol{\gamma} \succeq \mathbf{0}, \end{aligned} \quad (39)$$

in which \mathbf{P} and \mathbf{b} are already defined in Lemma 2. In order to analyze the property of the minimization problem (39), we

introduce a symmetric matrix $\mathbf{Z} \in \mathbb{R}^{M \times M}$ here. Therefore, the problem with respect to \mathbf{Z} and $\boldsymbol{\gamma}$ becomes

$$\min_{\mathbf{Z}, \boldsymbol{\gamma}} \quad \log \det \mathbf{Z} \quad (a.1)$$

$$\text{s. t.} \quad \mathbf{Z} \succeq \boldsymbol{\Phi} \Sigma_0 \boldsymbol{\Phi}^T \quad (a.2)$$

$$\mathbf{P}(\sqrt{\boldsymbol{\gamma}} \otimes \sqrt{\boldsymbol{\gamma}}) = \mathbf{b} \quad (a.3)$$

$$\boldsymbol{\gamma} \succeq \mathbf{0}, \quad (a.4)$$

It is evident that problem (39) and problem (a) are equivalent. Denote the solution of (a) as $(\mathbf{Z}^*, \boldsymbol{\gamma}^*)$, so $\boldsymbol{\gamma}^*$ here is also the solution of (39). Thus, we will analysis the minimization problem (a) instead in the following paragraph.

We first demonstrate the concavity of (a). Obviously, with respect to \mathbf{Z} and $(\sqrt{\boldsymbol{\gamma}} \otimes \sqrt{\boldsymbol{\gamma}})$, the objective function $\log \det \mathbf{Z}$ is concave, and (a.3) is convex. Hence, we only need to show the convexity of (a.2) and (a.4) with respect to \mathbf{Z} and $(\sqrt{\boldsymbol{\gamma}} \otimes \sqrt{\boldsymbol{\gamma}})$.

It is observed that

$$\boldsymbol{\gamma} = \begin{pmatrix} \mathbf{h}_1^T & & & \\ & \mathbf{h}_2^T & & \\ & & \ddots & \\ & & & \mathbf{h}_{gL}^T \end{pmatrix} (\sqrt{\boldsymbol{\gamma}} \otimes \sqrt{\boldsymbol{\gamma}}) \triangleq \mathbf{H}(\sqrt{\boldsymbol{\gamma}} \otimes \sqrt{\boldsymbol{\gamma}}),$$

where $\mathbf{h}_i \triangleq (\delta_{i1}, \dots, \delta_{i,gL})^T$, $\mathbf{H} \in \mathbb{R}^{gL \times (gL)^2}$. Based on lemma 1 and the convexity-preserving property of linear transformation [33], $\mathbf{Z} \succeq \boldsymbol{\Phi} \Sigma_0 \boldsymbol{\Phi}^T$ is also convex with respect to \mathbf{Z} and $(\sqrt{\boldsymbol{\gamma}} \otimes \sqrt{\boldsymbol{\gamma}})$. Similarly, the constraint $\boldsymbol{\gamma} \succeq \mathbf{0}$ exhibits convexity. Therefore, (a) is concave with respect to $(\sqrt{\boldsymbol{\gamma}} \otimes \sqrt{\boldsymbol{\gamma}})$ and \mathbf{Z} . So we can rewrite (a) as

$$\begin{aligned} \min_{\mathbf{Z}, \sqrt{\boldsymbol{\gamma}} \otimes \sqrt{\boldsymbol{\gamma}}} \quad & \log \det \mathbf{Z} \\ \text{s. t.} \quad & \mathbf{Z} \succeq \boldsymbol{\Phi} \Sigma_0 \boldsymbol{\Phi}^T \\ & \mathbf{P}(\sqrt{\boldsymbol{\gamma}} \otimes \sqrt{\boldsymbol{\gamma}}) = \mathbf{b} \\ & \boldsymbol{\gamma} \succeq \mathbf{0}. \end{aligned} \quad (b)$$

The minimum of (b) will achieve at an extreme point. According to the equivalence between extreme point and basic feasible solution (BFS) [34], the extreme point of (b) is a BFS to

$$\begin{cases} \mathbf{Z} \succeq \boldsymbol{\Phi} \Sigma_0 \boldsymbol{\Phi}^T \\ \mathbf{P}(\sqrt{\boldsymbol{\gamma}} \otimes \sqrt{\boldsymbol{\gamma}}) = \mathbf{b} \\ \boldsymbol{\gamma} \succeq \mathbf{0} \end{cases},$$

which concludes $\|\sqrt{\boldsymbol{\gamma}} \otimes \sqrt{\boldsymbol{\gamma}}\|_0 \leq r(\mathbf{P}) = M$, equivalently $\|\boldsymbol{\gamma}\|_0 \leq \sqrt{M}$. This result implies that every local minimum (also a BFS to the convex polytope) must be attained at a sparse solution. \square

It is worth noting that in Theorem 2, we have assumed a noise-free scenario ($\beta \rightarrow \infty$). In general, we conjecture that similar conclusion may hold even in the presence of noise.

V. EXPERIMENTS

In this section, we compare DivSBL with the following six algorithms:

- Block-Based: BSBL, Group Lasso, Group BPDN.
- Pattern-Based: PC-SBL, StructOMP.

TABLE I
RECONSTRUCTION ERROR OF THE SYNTHETIC SIGNAL DATA SETS.

ALGORITHM	HOMO-NMSE	HETERO-NMSE	BETTER?
BSBL	0.0172	0.0261	×
PC-SBL	0.0915	0.0790	✓
SBL	0.0441	0.0533	×
GROUP LASSO	0.0233	0.1357	×
GROUP BPDN	0.0598	0.1406	×
STRUCTOMP	0.0674	0.0563	✓
DIVSBL	0.0112	0.0087	✓

- Sparse learning (without structural information): SBL.

The following results are obtained by averaging over 100 random runs, and the signal-to-noise ratio (SNR) is 15 dB unless otherwise specified. The full signal dimension is denoted as N , and the number of measurements is denoted as M . Normalized Mean Squared Error (NMSE), defined as $\|\hat{x} - x_{\text{true}}\|_2 / \|x_{\text{true}}\|_2$, is used as a measure to compare different algorithms.

For reproducibility, the experiment code is available in <https://github.com/YanhaoZhang1/DivSBL>.

A. Synthetic Signal Data

We first test on synthetic signal data. The experimental result on homoscedastic data provided by [23], which is served as a special case of heteroscedastic data, is provided in Appendix B. In this subsection, the algorithms are evaluated on heteroscedastic signal data, which allows for arbitrary block pattern. This implies that the block size, non-zero quantity, block location, and variance of the signals to be recovered are generated randomly, offering a pattern that is more representative of real-world data.

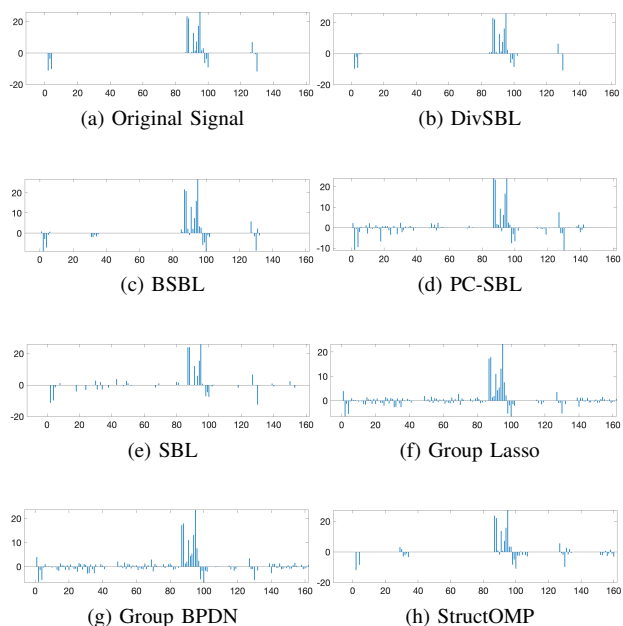


Fig. 4. The original **heteroscedastic** signal and reconstructed results by respective algorithms. ($N = 162$, $M = 80$)

TABLE II
RECONSTRUCTION ERROR (NMSE) ACROSS VARIOUS PRE-DEFINED BLOCK SIZES. (TO SIMPLIFY NOTATION, WE REFER TO GROUP LASSO AS ‘G-LASSO’ AND GROUP BPDN AS ‘G-BPDN’ IN THIS TABLE.)

BLOCKSIZE	BSBL	G-LASSO	G-BPDN	DIVSBL
2	0.0425	0.0707	0.0846	0.0417
3	0.0399	0.0702	0.0824	0.0335
6	0.0224	0.0717	0.0791	0.0120
9	0.0580	0.1155	0.1174	0.0392
18	0.2385	0.2593	0.2650	0.0579
54	0.4550	0.4021	0.4082	0.0676
162	0.4960	0.5315	0.5318	0.0822
MEAN	0.2155	0.1915	0.2149	0.0481

Figure 4 and the third column of Table I present the reconstruction results. DivSBL surpasses other algorithms by **more than 66.7%**, showcasing a substantial performance enhancement.

It’s also worth noting that we specifically control the same number of non-zero elements on homoscedastic data in Appendix B, and compress with the same ratio under identical environmental noise. Apart from our algorithm, other block-based algorithms exhibit a performance decline. Although our algorithm belongs to block-based algorithm, this result indicates that DivSBL is able to overcome the limitation of such algorithms. The next subsection will further highlight our advantages compared to other block-based algorithms.

B. The Robustness of Pre-defined Block Sizes

As mentioned in Section I, the block-based algorithms require setting the size of blocks in advance, and the performance is sensitive to the preset parameter, which is challenging in practice.

This experiment tests the robustness performance of block-based algorithms with pre-defined block sizes. The signal dimension here is $N = 162$, and we set the preset block sizes to 2, 3, 6, 9, 18, 54, and 162, respectively. The reconstruction error is shown in Figure 5 and Table II. For varying preset block sizes, DivSBL demonstrates an average improvement of **over 74.9%** compared to other algorithms.

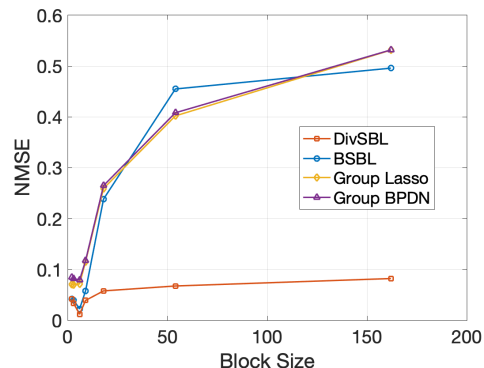


Fig. 5. NMSE variation with changing preset block sizes.

The result indicates that DivSBL demonstrates strong robustness to the preset block sizes, effectively addressing the sensitivity issue that block-based algorithms commonly encounter with respect to block sizes. Subsequent tests on real datasets further validate the effectiveness of our model and algorithm.

C. 1D AudioSet

Audio signals exhibit block sparse structures in discrete cosine transform (DCT) basis. As shown in Figure 6, the original audio signal (a) exhibits clustered sparse structure (b) after DCT transformation, which is well-suited for assessing block sparse algorithms.

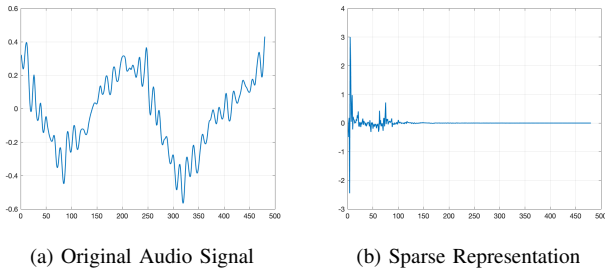


Fig. 6. The original signal and its sparse representation.

In this subsection, we carry out experiments on real-world audio signal, which is randomly chosen in *AudioSet*³ [35]. The reconstruction results are present in Figure 7. It is noteworthy that DivSBL exhibits an improvement of **over 24.2%** compared to other algorithms.

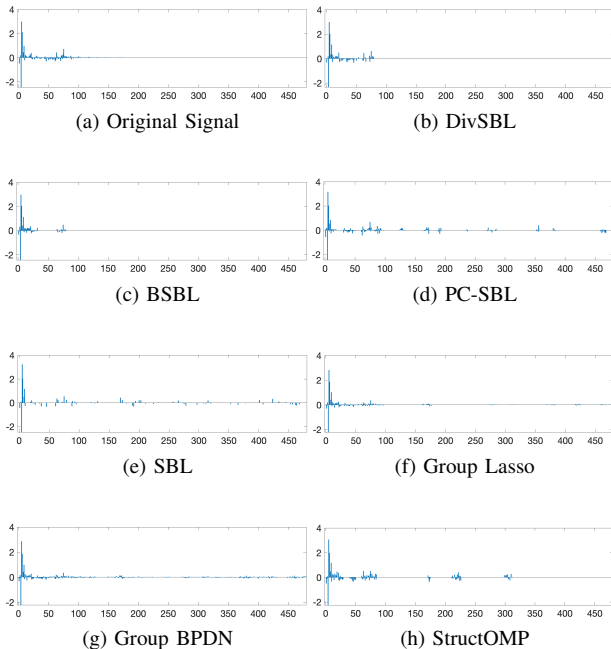


Fig. 7. The sparse audio signal reconstructed by respective algorithms. NMSE: (b) **0.0406** (c) 0.0572 (d) 0.1033 (e) 0.1004 (f) 0.0536 (g) 0.0669 (h) 0.1062. ($N = 480, M = 150$)

³Available at <https://research.google.com/audioset/>.

D. The Sensitivity of Sample Rate

In this experiment, the algorithms are tested on real-life audio data introduced before to investigate the sensitivity of sample rate (M/N) varied from 0.25 to 0.55. The result is visualized in Figure 8. Notably, DivSBL algorithm emerges as the top performer across diverse sampling rates, displaying a consistent enhancement of around 1 dB in NMSE compared to the best-performing algorithm among others.

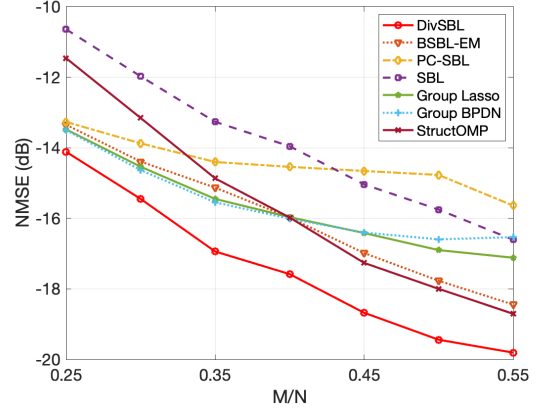


Fig. 8. NMSE vs. Sample rate of respective algorithms.

E. 2D Image Reconstruction

In 2D image experiments, we utilize a standard set of grayscale images compiled from two sources⁴.

As depicted in Figure 9, the images exhibit block sparsity in discrete wavelet domain. Therefore, real-world images also serve as a proper scenario for testing block sparse algorithms.

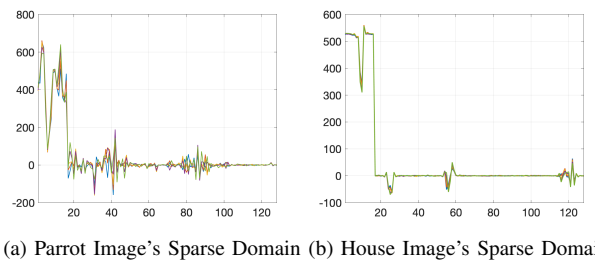


Fig. 9. Parrot and House image data (the first five columns) transformed in wavelet domain.

In Section V-D, we have substantiated the superior performance of DivSBL across diverse sampling rates. In this experiment, we use a sample rate of 0.5 to test different block sparse algorithms on various real-world images. The reconstruction errors are present in Table III. DivSBL yields superior quality reconstructions than other algorithms, achieving an average improvement of **around 7%** on different images.

In Figures 10 and 11, we display the final reconstructions of Parrot and House images as examples. From Figure 10,

⁴Available at <http://dsp.rice.edu/software/DAMP-toolbox> and http://see.xidian.edu.cn/faculty/wsdong/NLR_Exps.htm.

TABLE III
RECONSTRUCTED ERROR (NMSE) OF THE TEST IMAGES.

ALG \ DATA	PARROT	CAMERAMAN	LENA	BOAT	HOUSE	BARBARA	MONARCH	FOREMAN
BSBL	0.1466	0.1572	0.1630	0.1750	0.1397	0.1460	0.2733	0.1203
PC-SBL	0.1292	0.1583	0.1524	0.1596	0.1424	0.1470	0.2139	0.1331
SBL	0.3528	0.4489	0.3991	0.1650	0.1685	0.1305	0.3729	0.1035
GROUP LASSO	0.1970	0.2090	0.2141	0.1453	0.1361	0.1299	0.2156	0.1170
GROUP BPDN	0.1964	0.2112	0.2143	0.1422	0.1329	0.1273	0.2159	0.1131
STRUCTOMP	0.1577	0.1839	0.2078	0.1915	0.1690	0.1790	0.2492	0.1581
DIVSBL	0.1190	0.1462	0.1407	0.1467	0.1176	0.1213	0.2117	0.0960

one can notice that DivSBL is capable of preserving the finer features of the parrot, such as cheek, eye, etc., and recovering the background smoothly with minimal error stripes. In Figure 11, nearly every reconstructed house introduces undesirable artifacts and stripes, while image restored by DivSBL shows the least amount of noise patterns, demonstrating the most effective restoration.

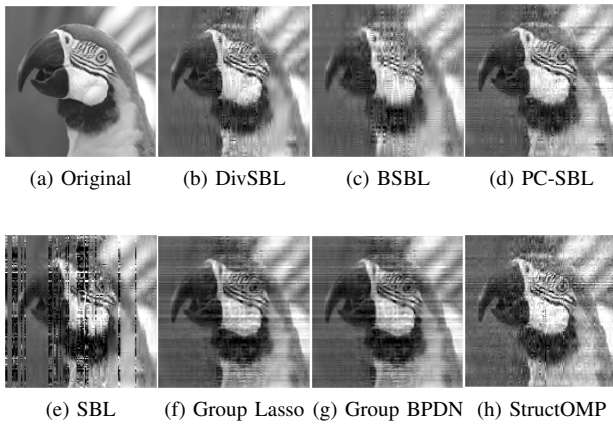


Fig. 10. Reconstruction results for Parrot image. (The corresponding NMSE is present in Table III.)

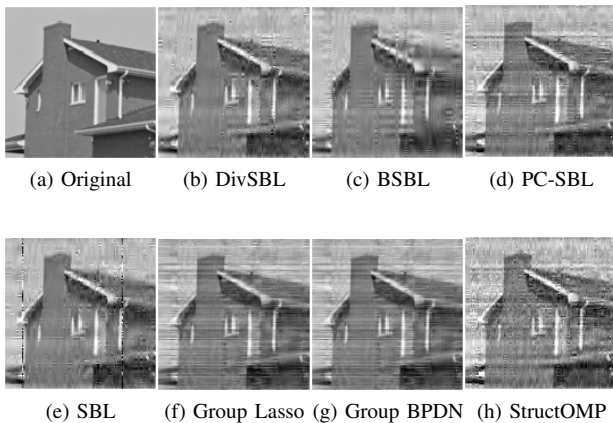


Fig. 11. Reconstruction results for House image. (The corresponding NMSE is present in Table III.)

VI. CONCLUSIONS

This paper established a new Bayesian learning model by introducing diversified block sparse prior, to effectively capture the prevalent block sparsity observed in real-world data. The novel Bayesian model effectively solved the sensitivity issue in existing block sparse learning methods, allowing for adaptive block estimation and reducing the risk of overfitting. The proposed algorithm DivSBL, based on this model, enjoyed solid theoretical guarantees on both convergence and sparsity theory. Experimental results demonstrated its state-of-the-art performance on multimodal data. Future works include exploration on more effective weak constraints for correlation matrices, and applications on supervised learning tasks such as regression and classification.

APPENDIX A

PROOF OF THEOREM 1

Proof. The posterior estimation of the block sparse signal is given by $\hat{\mathbf{x}} = \beta \hat{\Sigma} \Phi^T \mathbf{y} = \left(\beta^{-1} \hat{\Sigma}_0^{-1} + \Phi^T \Phi \right)^{-1} \Phi^T \mathbf{y}$, where $\hat{\Sigma}_0 = \text{diag} \left\{ \hat{\mathbf{G}}_1 \hat{\mathbf{B}}_1 \hat{\mathbf{G}}_1, \hat{\mathbf{G}}_2 \hat{\mathbf{B}}_2 \hat{\mathbf{G}}_2, \dots, \hat{\mathbf{G}}_g \hat{\mathbf{B}}_g \hat{\mathbf{G}}_g \right\}$, and $\hat{\mathbf{G}}_i = \text{diag} \left\{ \sqrt{\hat{\gamma}_{i1}}, \dots, \sqrt{\hat{\gamma}_{iL}} \right\}$.

Let $\hat{\gamma} = (\hat{\gamma}_{11}, \dots, \hat{\gamma}_{1L}, \dots, \hat{\gamma}_{g1}, \dots, \hat{\gamma}_{gL})^T$, which is obtained by globally minimizing (40) for a given $\hat{\mathbf{B}}_i$ ($\forall i$).

$$\min_{\gamma} \mathcal{L}(\gamma) = \mathbf{y}^T \Sigma_y^{-1} \mathbf{y} + \log \det \Sigma_y. \quad (40)$$

Inspired by [36], we can rewrite the first summation term as

$$\mathbf{y}^T \Sigma_y^{-1} \mathbf{y} = \min_{\mathbf{x}} \left\{ \beta \|\mathbf{y} - \Phi \mathbf{x}\|_2^2 + \mathbf{x}^T \Sigma_0^{-1} \mathbf{x} \right\}.$$

Then (40) is equivalent to

$$\begin{aligned} \min_{\gamma} \mathcal{L}(\gamma) &= \min_{\gamma} \left\{ \min_{\mathbf{x}} \left\{ \beta \|\mathbf{y} - \Phi \mathbf{x}\|_2^2 + \mathbf{x}^T \Sigma_0^{-1} \mathbf{x} \right\} + \log \det \Sigma_y \right\} \\ &= \min_{\mathbf{x}} \left\{ \min_{\gamma} \left\{ \mathbf{x}^T \Sigma_0^{-1} \mathbf{x} + \log \det \Sigma_y \right\} + \beta \|\mathbf{y} - \Phi \mathbf{x}\|_2^2 \right\}. \end{aligned}$$

So when $\beta \rightarrow \infty$, (40) is equivalent to minimizing the following problem,

$$\begin{aligned} \min_{\mathbf{x}} \left\{ \min_{\gamma} \left\{ \mathbf{x}^T \Sigma_0^{-1} \mathbf{x} + \log \det \Sigma_y \right\} \right\} \\ \text{s. t. } \mathbf{y} = \Phi \mathbf{x}. \end{aligned} \quad (41)$$

Let $g(\mathbf{x}) = \min_{\gamma} \left\{ \mathbf{x}^T \Sigma_0^{-1} \mathbf{x} + \log \det \Sigma_y \right\}$, then according to Lemma 1 in [36], $g(\mathbf{x})$ satisfies

$$g(\mathbf{x}) = \mathcal{O}(1) + [M - \min(M, KL)] \log \beta^{-1},$$

where K represents the estimated number of blocks and $\beta^{-1} \rightarrow 0$ (noiseless). Therefore, when $g(\mathbf{x})$ achieves its minimum value by (41), K will achieve its minimum value simultaneously.

The results in [37] demonstrate that if $K_0 < \frac{M+1}{2L}$, then no other solution exists such that $\mathbf{y} = \Phi\mathbf{x}$ with $K < \frac{M+1}{2L}$. Therefore, we have $K \geq K_0$, and when K reaches its minimum value K_0 , the estimated signal $\hat{\mathbf{x}} = \mathbf{x}_{\text{true}}$. \square

APPENDIX B

THE EXPERIMENT OF 1D HOMOSCEDASTIC SIGNALS WITH BLOCK SPARSITY

As mentioned in Section II-A3, homoscedasticity can be seen as a special case of our model. Therefore, we test our algorithm on homoscedastic data provided in [23]. In this dataset, each block shares the same size $L = 6$, and the amplitudes within each block follow a homoscedastic normal distribution.

The reconstructed results are shown in Figure 12 and the second column of Table I. DivSBL demonstrates a remarkable improvement of **over 34.9%** compared to other algorithms.

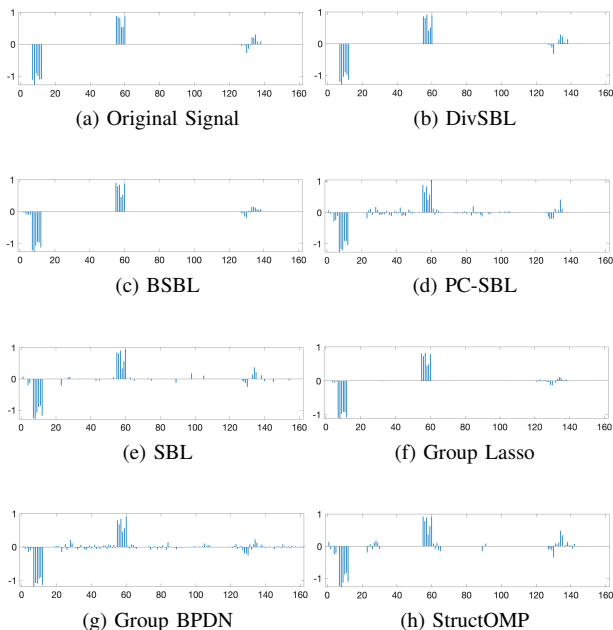


Fig. 12. The original **homoscedastic** signal and reconstructed results by respective algorithms. ($N = 162, M = 80$)

REFERENCES

- [1] David L Donoho. Compressed sensing. *IEEE Transactions on information theory*, 52(4):1289–1306, 2006.
- [2] Irina F Gorodnitsky and Bhaskar D Rao. Sparse signal reconstruction from limited data using FOCUSS: A re-weighted minimum norm algorithm. *IEEE Transactions on signal processing*, 45(3):600–616, 1997.
- [3] Emmanuel J Candes and Terence Tao. Decoding by linear programming. *IEEE transactions on information theory*, 51(12):4203–4215, 2005.
- [4] Robert Tibshirani. Regression shrinkage and selection via the lasso. *Journal of the Royal Statistical Society Series B: Statistical Methodology*, 58(1):267–288, 1996.
- [5] Michael E Tipping. Sparse Bayesian learning and the relevance vector machine. *Journal of machine learning research*, 1(Jun):211–244, 2001.

- [6] Scott Shaobing Chen, David L Donoho, and Michael A Saunders. Atomic decomposition by basis pursuit. *SIAM review*, 43(1):129–159, 2001.
- [7] Yagyensh Chandra Pati, Ramin Rezaifar, and Perinkulam Sambamurthy Krishnaprasad. Orthogonal matching pursuit: Recursive function approximation with applications to wavelet decomposition. In *Proceedings of 27th Asilomar conference on signals, systems and computers*, pages 40–44. IEEE, 1993.
- [8] Jian Zhang and Bernard Ghanem. Ista-net: Interpretable optimization-inspired deep network for image compressive sensing. In *Proceedings of the IEEE conference on computer vision and pattern recognition*, pages 1828–1837, 2018.
- [9] Zi-En Fan, Feng Lian, and Jia-Ni Quan. Global sensing and measurements reuse for image compressed sensing. In *Proceedings of the IEEE/CVF Conference on Computer Vision and Pattern Recognition*, pages 8954–8963, 2022.
- [10] Yonina C Eldar, Patrick Kuppinger, and Helmut Bolcskei. Block-sparse signals: Uncertainty relations and efficient recovery. *IEEE Transactions on Signal Processing*, 58(6):3042–3054, 2010.
- [11] David L Donoho, Iain Johnstone, and Andrea Montanari. Accurate prediction of phase transitions in compressed sensing via a connection to minimax denoising. *IEEE transactions on information theory*, 59(6):3396–3433, 2013.
- [12] Charlie Nash, Jacob Menick, Sander Dieleman, and Peter Battaglia. Generating images with sparse representations. In *International Conference on Machine Learning*, pages 7958–7968. PMLR, 2021.
- [13] Darshan Thaker, Paris Giampouras, and René Vidal. Reverse engineering l_p attacks: A block-sparse optimization approach with recovery guarantees. In *International Conference on Machine Learning*, pages 21253–21271. PMLR, 2022.
- [14] Yuchen Fan, Jiahui Yu, Yiqun Mei, Yulun Zhang, Yun Fu, Ding Liu, and Thomas S Huang. Neural sparse representation for image restoration. *Advances in Neural Information Processing Systems*, 33:15394–15404, 2020.
- [15] Peng Jiang, Lihan Hu, and Shihui Song. Exposing and exploiting fine-grained block structures for fast and accurate sparse training. *Advances in Neural Information Processing Systems*, 35:38345–38357, 2022.
- [16] Mehdi Korki, Jingxin Zhang, Cishen Zhang, and Hadi Zayyani. Block-sparse impulsive noise reduction in OFDM systems—a novel iterative Bayesian approach. *IEEE Transactions on Communications*, 64(1):271–284, 2015.
- [17] Aditya Sant, Markus Leinonen, and Bhaskar D Rao. Block-sparse signal recovery via general total variation regularized sparse Bayesian learning. *IEEE Transactions on Signal Processing*, 70:1056–1071, 2022.
- [18] Ming Yuan and Yi Lin. Model selection and estimation in regression with grouped variables. *Journal of the Royal Statistical Society Series B: Statistical Methodology*, 68(1):49–67, 2006.
- [19] Francis R Bach. Consistency of the group lasso and multiple kernel learning. *Journal of Machine Learning Research*, 9(6), 2008.
- [20] Laurent Jacob, Guillaume Obozinski, and Jean-Philippe Vert. Group lasso with overlap and graph lasso. In *Proceedings of the 26th annual international conference on machine learning*, pages 433–440, 2009.
- [21] Ewout Van Den Berg and Michael P Friedlander. Probing the Pareto frontier for basis pursuit solutions. *SIAM journal on scientific computing*, 31(2):890–912, 2009.
- [22] Zhilin Zhang and Bhaskar D Rao. Sparse signal recovery with temporally correlated source vectors using sparse Bayesian learning. *IEEE Journal of Selected Topics in Signal Processing*, 5(5):912–926, 2011.
- [23] Zhilin Zhang and Bhaskar D Rao. Extension of sbl algorithms for the recovery of block sparse signals with intra-block correlation. *IEEE Transactions on Signal Processing*, 61(8):2009–2015, 2013.
- [24] Zhilin Zhang and Bhaskar D Rao. Recovery of block sparse signals using the framework of block sparse bayesian learning. In *2012 IEEE International Conference on Acoustics, Speech and Signal Processing (ICASSP)*, pages 3345–3348. IEEE, 2012.
- [25] Junzhou Huang, Tong Zhang, and Dimitris Metaxas. Learning with structured sparsity. In *Proceedings of the 26th Annual International Conference on Machine Learning*, pages 417–424, 2009.
- [26] Jun Fang, Yanning Shen, Hongbin Li, and Pu Wang. Pattern-coupled sparse Bayesian learning for recovery of block-sparse signals. *IEEE Transactions on Signal Processing*, 63(2):360–372, 2014.
- [27] Lu Wang, Lifan Zhao, Susanto Rahardja, and Guoan Bi. Alternative to extended block sparse Bayesian learning and its relation to pattern-coupled sparse Bayesian learning. *IEEE Transactions on Signal Processing*, 66(10):2759–2771, 2018.

- [28] Jisheng Dai, An Liu, and Hing Cheung So. Non-uniform burst-sparsity learning for massive MIMO channel estimation. *IEEE Transactions on Signal Processing*, 67(4):1075–1087, 2018.
- [29] David JC MacKay. Bayesian interpolation. *Neural computation*, 4(3):415–447, 1992.
- [30] Arthur P Dempster, Nan M Laird, and Donald B Rubin. Maximum likelihood from incomplete data via the EM algorithm. *Journal of the royal statistical society: series B (methodological)*, 39(1):1–22, 1977.
- [31] Stephen P Boyd and Lieven Vandenberghe. *Convex optimization*. Cambridge university press, 2004.
- [32] David P Wipf and Bhaskar D Rao. Sparse Bayesian learning for basis selection. *IEEE Transactions on Signal processing*, 52(8):2153–2164, 2004.
- [33] Ralph Tyrell Rockafellar. *Convex Analysis*. Princeton University Press, 1970.
- [34] David G Luenberger and Yinyu Ye. *Linear and nonlinear programming*, volume 116. Springer, 2008.
- [35] Jort F Gemmeke, Daniel PW Ellis, Dylan Freedman, Aren Jansen, Wade Lawrence, R Channing Moore, Manoj Plakal, and Marvin Ritter. Audio set: An ontology and human-labeled dataset for audio events. In *2017 IEEE international conference on acoustics, speech and signal processing (ICASSP)*, pages 776–780. IEEE, 2017.
- [36] David P Wipf, Julia P Owen, Hagai T Attias, Kensuke Sekihara, and Srikantan S Nagarajan. Robust Bayesian estimation of the location, orientation, and time course of multiple correlated neural sources using MEG. *NeuroImage*, 49(1):641–655, 2010.
- [37] Shane F Cotter, Bhaskar D Rao, Kjersti Engan, and Kenneth Kreutz-Delgado. Sparse solutions to linear inverse problems with multiple measurement vectors. *IEEE Transactions on signal processing*, 53(7):2477–2488, 2005.